ELSEVIER

Contents lists available at ScienceDirect

Ecological Indicators

journal homepage: www.elsevier.com/locate/ecolind





Assessing the impact of urban block-scale landscape features on the diurnal cooling of green spaces using SDGSAT-1*

Chang Liu^a, Xiaoying Ouyang ^{b,c}, Jinxin Yang ^d, Dinoo Gunasekera ^{b,c}, Qihao Weng ^{e,f,g}, Xuesheng Zhao^a, Zhongchang Sun ^{b,c,*}

- a College of Geoscience and Surveying Engineering, China University of Mining and Technology-Beijing, Beijing 100083, China
- b International Research Center of Big Data for Sustainable Development Goals, Beijing 100094, China
- ^c Aerospace Information Research Institute, Chinese Academy of Sciences, Beijing 100094, China
- ^d School of Geography and Remote Sensing, Guangzhou University, Guangzhou 510006, China
- e JC STEM Lab of Earth Observations, Department of Land Surveying and Geo-Informatics, The Hong Kong Polytechnic University, Hung Hom, Hong Kong
- f Research Centre for Artificial Intelligence in Geomatics, The Hong Kong Polytechnic University, Hung Hom, Hong Kong
- g Research Institute for Land and Space, The Hong Kong Polytechnic University, Hung Hom, Hong Kong

ARTICLE INFO

Keywords: Sustainable Development Goal (SDG) Urban green space Diurnal cooling effect SDGSAT-1 Boosted regression tree Landscape features

ABSTRACT

Urban green space (UGS) is a key component of Sustainable Development Goal (SDG) 11.7.1, urban public open space, and is essential for mitigating the urban heat island (UHI) effect. However, the impact of urban landscape features on the diurnal cooling performance of UGS at the block scale across different climates remains insufficiently understood. The objective of this study is to explore the differences in features that influence the cooling intensity of UGS at both day and night under varying climatic conditions. Four Chinese cities located in distinct climate zones—Beijing, Shanghai, Haikou, and Urumqi—were selected as study areas. High-resolution land surface temperature (LST) data for summer days and nights were derived from SDGSAT-1/TIS imagery, while land cover classifications were obtained from Gaofen (GF) satellite images. UGS cooling intensity was calculated as the temperature difference between impervious surfaces and UGS within each urban block. To identify the key metrics influencing UGS cooling, we employed a boosted regression tree (BRT) model incorporating seven UGS landscape metrics, one UGS biophysical metric, and four urban block morphology metrics. The results revealed that UGS exhibited a more pronounced cooling effect during the daytime than at night. Key metrics also varied across cities. During the day, UGS area (+), UGS edge density (-), and block patch density (-) were significant in Beijing and Shanghai, while block area (+), UGS aggregation index (+), and UGS edge density (-) were dominant in Haikou and Urumqi. At night, the UGS aggregation index (+) was the most influential metric across all four cities. Moreover, the key metrics exhibited optimal values or thresholds of influence, with significant differences observed across cities. This study provides an important insight into how UGS features regulate diurnal cooling across different climates and offers recommendations for UHI mitigation strategies.

1. Introduction

In the context of global urbanization, the extensive replacement of natural surfaces with artificial ones has disrupted the surface energy balance and triggered the Urban Heat Island (UHI) effect, which is characterized by higher Land Surface Temperature (LST) in urban centers compared to suburban areas (Zargari et al., 2024; Chen et al., 2023). As global warming intensifies, the frequency and severity of urban heatwaves are projected to increase (He et al., 2022; Marcotullio et al.,

2022; Barriopedro et al., 2023), amplifying UHI effects and placing additional strain on urban systems. Consequently, identifying cost-effective strategies for UHI mitigation and enhancing urban thermal comfort has become imperative.

The Sustainable Development Goals (SDGs), adopted by the United Nations as part of the 2030 Agenda (Guo et al., 2022; Jiang et al., 2021), emphasize the importance of enhancing the accessibility and functionality of urban green space (UGS), which provide an effective solution for mitigate the UHI effect. Numerous studies have demonstrated that UGS

https://doi.org/10.1016/j.ecolind.2025.113937

Received 22 April 2025; Received in revised form 13 July 2025; Accepted 22 July 2025 Available online 26 July 2025

 $^{^{\}star}$ This article is part of a special issue entitled: 'NbS for Holistic Management' published in Ecological Indicators.

^{*} Corresponding author at: International Research Center of Big Data for Sustainable Development Goals, Beijing 100094, China. E-mail address: sunzc@aircas.ac.cn (Z. Sun).

plays a crucial role in regulating localized urban climates (Athokpam et al., 2024; Li et al., 2023b; Liu et al., 2023; Wang et al., 2022). UGS effectively reduces LST through mechanisms such as shading, solar radiation absorption, and transpiration (Yu et al., 2024; Bakhshoodeh et al., 2022), with temperature differences of up to 5.44 °C observed between UGS and impervious surfaces (Khan and Li, 2024). Additionally, the configuration and structural characteristics of UGS significantly influence its cooling effect (Nie et al., 2024; Rakoto et al., 2021). UGSs with multiple vegetation types exhibit more significant cooling effects than those consisting of a single vegetation type (Wei et al., 2025). Furthermore, research has shown that UGS landscape metrics, biophysical metrics, and urban block morphology metrics play crucial roles in regulating LST (Bai et al., 2024; Hu et al., 2022; Tehrani et al., 2024). Regarding landscape metrics, the area, patch density, and shape of UGS significantly influence LST (Li et al., 2023c; Liu et al., 2024; Nasar-u-Minallah et al., 2024). Similarly, the edge density, coverage, and aggregation index of UGS are negatively correlated with LST (Cui et al., 2024; Wang et al., 2023). In terms of biophysical metrics, the normalized difference vegetation index (NDVI) is typically negatively correlated with LST (Guha and Govil, 2021). Concerning urban block morphology metrics, block shape, patch density, and diversity indices may also influence LST (Zhou et al., 2014).

Recent studies have highlighted the importance of incorporating the spatial and temporal heterogeneity of UHI effects into urban planning and governance. Green infrastructure, such as green roofs and urban ventilation corridors, has proven effective in mitigating UHI through cooling and airflow enhancement (Dong et al., 2024; Guo et al. (2023a), Guo et al. (2023b)). However, the cooling effect of UGS varies significantly across different climatic conditions. In humid climates, higher air humidity and adequate water supply promote vegetation growth and enhance transpiration, effectively reducing LST (Zhu et al., 2023). In contrast, in arid or semi-arid regions, the transpiration cooling effect of vegetation is limited due to restricted water availability, resulting in a diminished cooling effect (Cheung et al., 2021). Land use changes,

especially increased impervious surfaces, further intensify UHI and highlight the need for coordinated blue-green space planning (Ren et al., 2024; Ren et al., 2023). In addition, population exposure and landscape patterns interact to produce fine-scale thermal heterogeneity, underscoring the importance of integrating human-air-ground coupling in planning strategies (Peng et al., 2024). While integration with water bodies enhances cooling (Shi et al., 2020), dense built environments may reduce effectiveness (Chen et al., 2024; Yang et al., 2024). Targeted greening, as in Chongqing, shows district-level cooling benefits (Wang et al., 2025), and irrigation strategies, particularly in the morning, improve lawn-based thermal performance via longwave radiation reduction (Huang and He, 2025). These findings establish a scientific foundation for UGS planning and support sustainable urban development. Furthermore, further exploration of the cooling potential of UGS will not only optimize urban planning but also enhance the comfort and health of residents.

Although the relationship between the cooling effect of UGS and urban landscape structure has become a prominent area of research, many aspects still require further investigation. First, selecting the appropriate spatial analysis unit is a critical consideration in this study. Conventional studies typically divide the study area into regular grids or utilize concentric buffers around a single UGS as the unit of analysis (Tan et al., 2021; Dong et al., 2022). While these methods are straightforward to implement, they often fail to fully capture the spatial heterogeneity of complex urban environments, including their structural and functional boundary characteristics. This limitation hinders an accurate assessment of the true impact of urban landscape features on the cooling effect of UGSs. Blocks are the fundamental units of a city, and due to the obstruction of heat flow by roads, they are often regarded as separate thermal zones (Yao et al., 2020; Sun et al., 2018). Recent studies have shown that 3D urban features, such as building height and tree density, significantly impact LST at the block scale, with trees providing a cooling effect during the day and buildings contributing to higher LST at night due to heat retention (Han et al., 2023; Han et al.,

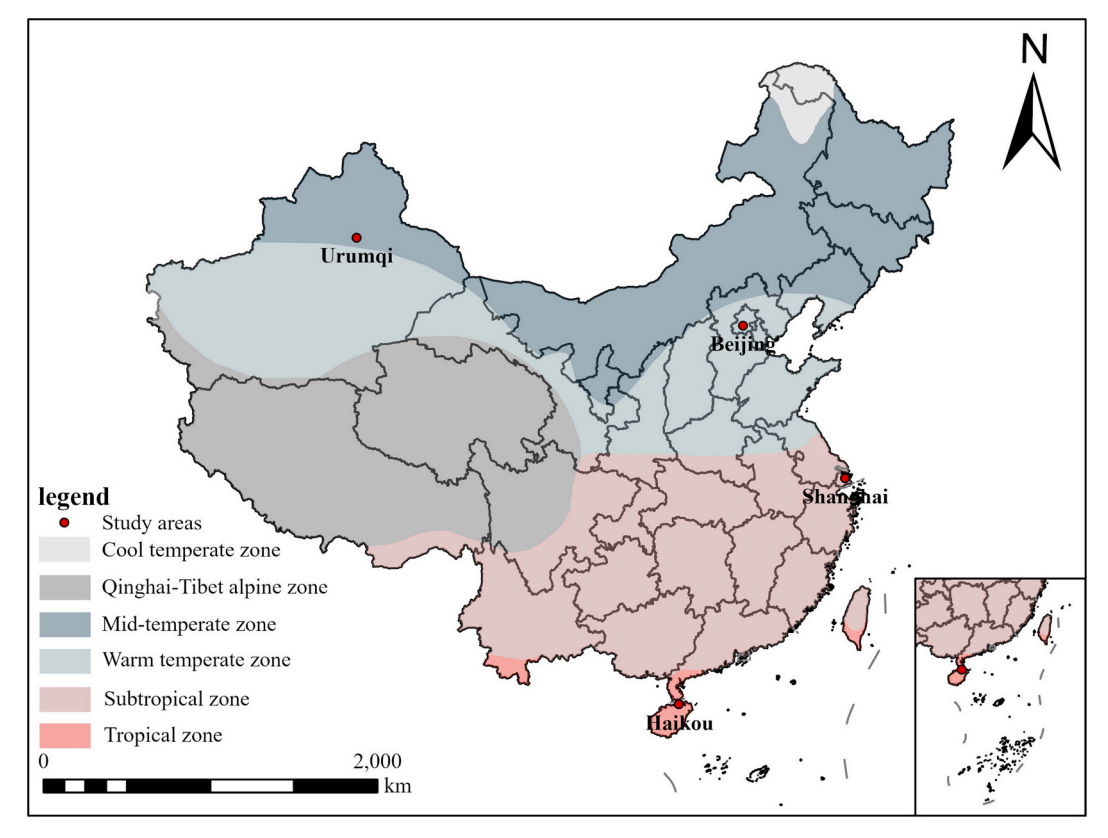


Fig. 1. Location of the study areas.

2024). However, the mechanisms influencing the cooling effect of UGS at the block scale remain unclear. Furthermore, much of the current research has focused on the cooling effects of UGS during the daytime (Shah et al., 2021; Ke et al., 2021), with relatively few studies addressing nighttime cooling mechanisms. At night, the cooling effect of UGS may be influenced by several factors, including radiative cooling and soil moisture. Research on the nighttime cooling effects of UGS is limited due to challenges related to the availability of nighttime LST remotely sensed imagery or its lower resolution (Arellano and Roca, 2021). In light of the growing urban nighttime heat island effect (Huang et al., 2021), a deeper understanding of the nighttime cooling mechanisms of UGS and their differences from daytime effects is essential for enhancing urban comfort and promoting resident health. Additionally, as global climate change intensifies and urban climate characteristics diversify (Esperon-Rodriguez et al., 2022; Yang and Zhao, 2024), conducting comparative studies of representative cities across various climate zones and systematically analyzing the factors influencing the cooling effect of UGS is crucial for developing climate-adapted urban landscape patterns. This research will provide valuable scientific evidence for addressing the challenges of UGS cooling across diverse climates worldwide.

The Sustainable Development Science Satellite 1 (SDGSAT-1) is the world's first scientific satellite dedicated to supporting the 2030 Agenda for Sustainable Development. It is equipped with a thermal infrared spectrometer (TIS) that can conduct both daytime and nighttime observations over a 24-hour period, providing high-resolution temperature data with continuous time-phase coverage (Guo et al. (2023a), Guo et al. (2023b)). This capability allows for the utilization of high-resolution temperature data to investigate the cooling effects of diurnal UGS. Furthermore, the SDGSAT-1 TIS captures images with a width of 300 km and has a revisit period of approximately 11 days (Li et al., 2023a). This enables the acquisition of LST data across various climatic contexts, facilitating the impact of how climatic differences influence the cooling effects of UGS. LST is essential for maintaining the surface energy balance (Li et al., 2020, Li et al., 2023d), and the capabilities of SDGSAT-1 provided the necessary data for this study. While conventional satellite and survey-based approaches often suffer from limited revisit frequency, low spatial resolution, or insufficient semantic richness, SDGSAT-1 enables more efficient and context-aware monitoring of urban thermal dynamics. By supporting consistent, fine-scale observations under varied climatic conditions, it enhances the reliability and interpretability of UGS cooling assessments, thereby reinforcing the methodological innovation of this study.

We selected four Chinese cities with distinct climatic backgrounds—Beijing, Shanghai, Haikou, and Urumqi—to develop climate zone-based diurnal strategies for UGS block-scale planning and management in a comparative study. We hypothesized that urban feature metrics exert differential effects on the cooling intensity of UGS under varying climatic conditions. The primary objectives of this study are as follows: (1) To investigate the daily variations in LST across different land covers in urban areas. (2) To identify the key feature metrics that influence the cooling effect of diurnal UGS at the block scale in the four representative cities. (3) To analyze the variations in the marginal effects of key diurnal metrics across the four representative cities. The findings provide practical recommendations for landscape optimization to mitigate the block-scale UHI effect across different climatic contexts.

2. Materials

2.1. Study areas

The study areas included Beijing, Shanghai, Haikou, and Urumqi. These four cities are located in distinct climate zones: Beijing in the warm temperate zone, Shanghai in the subtropical zone, Haikou in the tropical zone, and Urumqi in the mid-temperate zone (Fig. 1). Beijing is located in northern China ($115^{\circ}25'-117^{\circ}30'E$, $39^{\circ}28'-41^{\circ}05'N$) with a total area of $16,410.54 \text{ km}^2$, and its resident population at the end of

Table 1
Data sources.

Name	Date (BJT)	Type	Data sources
Built-up areas datasets	2020	Vector	A dataset of built-up areas of Chinese cities in 2020, (http://www. https://doi.org/10.11922/sciencedb. j00001.00332)
Road network data	June 2024	Vector	Open Street Map (OSM), (https://www.openstreetmap.org/)
GF satellite image	Beijing: Aug 23, 2023 Shanghai: Oct 2, 2022 Haikou: Aug 2, 2024 Aug 17, 2023 Urumqi: Aug 24, 2022	Raster	CRESDA, (https://data.cresda. cn/#/2dMap)
SDGSAT-1/ TIS	Beijing: Sept 14, 2023 (10:08)	Raster	International Research Center of Big Data for Sustainable Development Goals (CBAS), (https://www.sdgsat.ac. cn/)
	Sept 6, 2023 (21:28) Shanghai: Aug 4,2024(09:38) Aug 23,2024 (21:03) Haikou: Sept 15, 2022 (10:28) Aug 27,2022 (21:59) Urumqi: Jul 16, 2024 (12:04) Jul 3, 2023		

Note: BJT, Beijing time.

2022 was 21.843 million. The city has a warm-temperate, semi-humid, semi-arid monsoon climate characterized by hot, rainy summers, cold, dry winters, and short springs and autumns. The average annual temperature in 2022 was 13.4 °C, with total precipitation measuring 585.4 mm (Beijing Municipal Bureau Statistics, 2023). Shanghai is situated in eastern China (120°52′-122°12′E, 30°40′-31°53′N), with a total area of 6,340.5 km², and its resident population at the end of 2022 was 24.7589 million. Shanghai features a subtropical monsoon climate with four distinct seasons, abundant sunshine, and significant rainfall. In 2022, the average annual temperature was 18 °C, with total precipitation reaching 1,044.1 mm (Shanghai Municipal Bureau Statistics, 2023). Haikou, located in southern China (110°07′-110°42′E, 19°31′-20°04′N), is the capital of Hainan Province, with a total area of approximately 2296.82 km², and its resident population at the end of 2022 was 2.9397 million. Haikou experiences a tropical monsoon maritime climate. The average annual temperature in 2022 was 24.5 °C, with total precipitation amount to 2,021.0 mm (Haikou Municipal Bureau Statistics, 2023). Urumqi, situated in northwestern China (86°37′-88°58′E, 42°45′-45°00′N), is the capital of the Xinjiang Uygur Autonomous Region, with a total area of approximately $13,800 \ \mathrm{km}^2$, and its resident population at the end of 2023 was 4.0848 million. The city has a semi-arid continental climate in the mid-temperate zone. (Urumqi Municipal Bureau Statistics, 2024). Beijing and Shanghai experience hot and rainy summers, Haikou has humid and hot summers, while Urumqi endures dry and hot summers.

2.2. Datasets

In our study, we collected and utilized various datasets, including

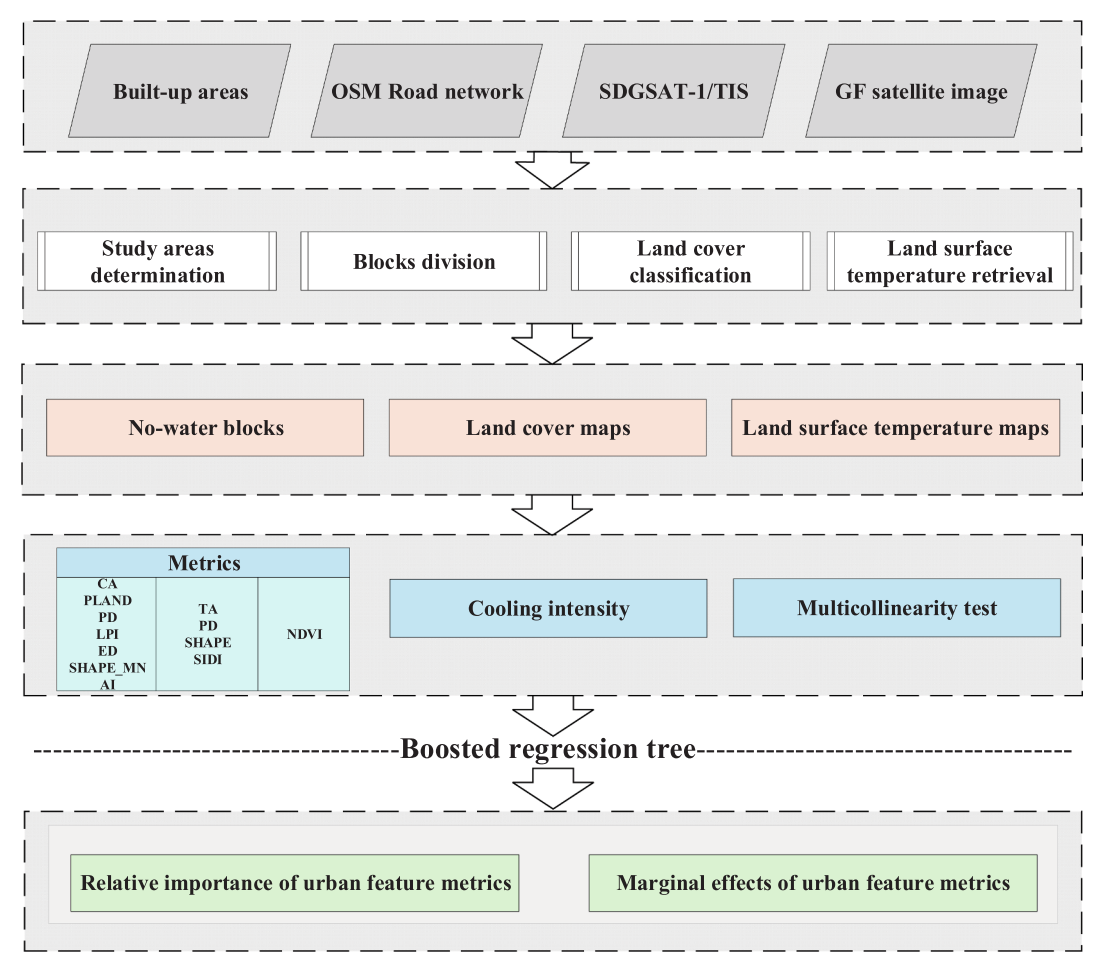


Fig. 2. Research flowchart.

urban built-up areas, road networks, Gaofen (GF) series satellite imagery, and diurnal SDGSAT-1/TIS imagery, as shown in Table 1.

Datasets of built-up areas were obtained from the Chinese Cities built-up areas datasets for 2020 (Sun et al., 2022) and were used to determine the extents of the study areas in the four cities. Road network data were sourced from OpenStreetMap (OSM) and utilized to segment urban blocks. This study employed cloud-free summer GF-6 satellite imagery for each city to map land cover. Additionally, SDGSAT-1/TIS imagery from the International Research Center of Big Data for Sustainable Development Goals (CBAS) was used to retrieve diurnal LSTs for the four cities. With a high spatial resolution of 30 m and three thermal infrared bands, the SDGSAT-1 TIS effectively monitors changes in LST, providing significant advantages, particularly in the analysis of temperature distributions in urban areas.

In this study, UGS primarily consists of forests, parks, and roadside green areas. The spatial resolution of the GF images is 2 m \times 2 m, while the spatial resolution of the LST data is 30 m \times 30 m. The LST data were resampled to a spatial resolution of 2 m \times 2 m to align with the land cover utilization data.

3. Methods

The flowchart shown in Fig. 2 outlines the methodology employed in this study. Initially, the GF image data for the four cities underwent preprocessing. Subsequently, land cover was categorized using the processed data. LSTs were then retrieved from SDGSAT-1/TIS imagery. Block segmentation was conducted utilizing OSM vector road network data. The cooling intensity of the UGS was analyzed at the block scale. Finally, the relationship between landscape metrics and cooling

intensity was examined. The following sections provide a detailed explanation of the methodology.

3.1. Block segmentation

This study utilized OSM vector road network maps to divide the blocks. Smaller blocks were merged to prevent them from being excessively small. Additionally, water-containing blocks were excluded to eliminate the influence of water bodies on the cooling effect of the UGS. Finally, a total of 3,148 blocks were included from Beijing, 2,386 from Shanghai, 1,045 from Haikou, and 1,449 from Urumqi in this study (Fig. 3).

3.2. Land cover classification

Based on GF imagery, an object-oriented algorithm was utilized to classify UGS, water-bodies, impervious surfaces, and bare land. Multi-resolution segmentation of the GF imagery was conducted using eCognition 10.3 software. This was followed by the selection of classification parameters, the establishment of classification rules, and the extraction of land cover classifications. The accuracy of the classification results was assessed using Google Earth as the reference standard, based on 300 randomly selected samples from each city.

3.3. LST retrieval

This study employed a modified temperature and emissivity separation (TES) algorithm to retrieve the LST and land surface emissivity (LSE) based on the three TIS bands of SDGSAT-1. Radiometric calibra-



Fig. 3. Spatial distribution of no-water blocks in four cities.

tion was initially conducted for the three bands, and digital number (DN) values were converted to radiance using the following equation:

$$L_{TOA} = DN*Gain + Bias (1)$$

 L_{TOA} denoted the top-of-atmosphere (TOA) radiance, expressed in $W/(m2 \cdot sr \cdot \mu m)$.

Next, atmospheric correction was performed for the three bands. The ERA5 atmospheric profile data were utilized, and the atmospheric parameters were processed using the radiative transfer model MODTRAN 5.2.2, which subsequently calculated the ground-leaving radiance (L_G). The following equation was employed, where τ was the atmospheric transmittance and L_u was the atmospheric upwelling radiance.

$$L_G = \frac{(L_{TOA} - L_u)}{\tau} \tag{2}$$

Finally, the LST was retrieved using the Planck function $(B(T_s))$ with the following equation, where T_s represented the LST, ε represented the LSE, and L_d represented the atmospheric downwelling radiance.

$$B(T_s) = \frac{L_G - (1 - \varepsilon)L_d}{c} \tag{3}$$

The accuracy of the temperature data retrieved using this method has been validated (Ouyang et al., 2024).

3.4. Cooling intensity calculation

Based on the classified UGS and impervious surfaces, the cooling intensity of the UGS at the block scale was calculated using the retrieved

LST data. The mean LST of the impervious surfaces within the block was subtracted from the mean LST of the UGS to determine the UGS cooling intensity (Yang et al., 2022).

$$T_{cooling} = \overline{T_B} - \overline{T_{ugs}} \tag{4}$$

Where $T_{cooling}$ was the cooling intensity of the UGS at the block scale, and $\overline{T_B}$ and $\overline{T_{ugs}}$ were the average LSTs of the impervious surfaces and the UGS within the block, respectively.

3.5. Urban feature metrics calculation

To comprehensively capture the urban characteristics that influence the cooling intensity of UGS and accurately identify the key metrics, this study selected seven class-level metrics related to UGS: class area (CA), percentage of landscape (PLAND), patch density (PD), largest patch index (LPI), edge density (ED), mean shape index (SHAPE_MN), and aggregation index (AI). Additionally, one biophysical metric, the normalized difference vegetation index (NDVI), was included to characterize UGS features. For urban blocks, four landscape-level metrics were chosen to describe block morphology: total area (TA), patch density (PD), shape index (SHAPE), and Simpson's diversity index (SIDI).

This study examined the impact of urban landscape features on the cooling effect of diurnal UGS under varying climatic conditions at the block scale. The research utilized 12 metrics, which included seven landscape metrics of UGS (CA_UGS, PLAND_UGS, PD_UGS, LPI_UGS, ED_UGS, SHAPE_MN_UGS, and AI_UGS), one biophysical metric (NDVI_UGS), and four urban block morphology metrics (TA_B, PD_B,

Table 2 Description of 12 metrics.

Category	Metrics	Formula	Abbreviation	Description of metric
UGS landscape metrics	Class area (ha)	$TA = \frac{\sum_{j=1}^{n_{i,j}} s_{i,j}}{10000}$	CA_UGS	Total area of UGS in urban block
	Percentage of landscape (%)	$\begin{array}{l} \text{PLAND} = \frac{\sum_{j=1}^{n_{i,u}} s_{i,j}}{S_i} \times 100 \end{array}$	PLAND_UGS	Percent coverage of UGS in urban block
	Patch density (number/100 ha)	$PD = \frac{n_{i,u}}{S_i} \times 10000 \times 100$	PD_UGS	Density of UGS patch in urban block
	Largest patch index (%)	$LPI = \frac{max(s_{i,j})}{S_i} \times 100$	LPI_UGS	The largest patch of UGS in urban block
	Edge density (m/ha)	$ ext{ED} = rac{\sum_{j=1}^{n_{lx}} e_{ij}}{\sum_{j=1}^{n_{lx}} s_{ij}}$	ED_UGS	Edge density of UGS patch in urban block
	shape index (–)	$SHAPE_MN = \frac{\sum_{j=1}^{n_{i,u}} 0.25e_{i,j}}{\sum_{j=1}^{n_{i,u}} \sqrt{s_{i,j}}}$	SHAPE_MN_UGS	Average landscape shape of UGS patch in urban block
	Aggregation index (%)	$AI = \left[\sum_{j=1}^{n_{i,n}} \left(\frac{g_{i,j}}{\max(g_{i,j})} \times PLAND_{i,j} \right) \right] \times 100$	AI_UGS	Aggregation level of UGS patch in urban block
UGS biophysical metric	Normalized difference vegetation index (–)	$NDVI = \frac{1}{a} \times \sum_{p=1}^{a} NDVI_p \ NDVI_p = $ $(NIR - R)/(NIR + R)$	NDVI_UGS	Coverage index of UGS in urban block
Urban block morphology metrics	Total area (ha)	$TA = \frac{S_i}{10000}$	TA_B	Total area of urban block
netres	Patch density (number /100 ha)	$PD = \frac{n_i}{S_i} \times 10000 \times 100$	PD_B	Density of land cover patches in urban block
	Shape index (–)	$SHAPE = \frac{0.25E_i}{\sqrt{S_i}}$	SHAPE_B	Landscape shape of urban block
	Simpson's diversity index (–)	$SIDI = 1 - \sum_{t=1}^{m} PLAND_t^2$	SIDI_B	Land cover patch uniformity of urban block

Note: $s_{i,j}$, $n_{i,u}$, $e_{i,j}$, $q_{i,j}$ denote the area of the jth UGS patch within the ith block, the total number of UGS patches within the ith block, the perimeter of the jth UGS patch within the ith block, and the number of neighboring UGS patches of the jth UGS patch within the ith block, respectively. a denotes the total number of pixels within the block. $NDVI_p$ denotes the NDVI value of the pth pixel within the block. NIR denotes the near-infrared band, and R denotes the red band. S_i , n_i , E_i , t, m denote the area of the ith block, the total number of patches within the ith block, the perimeter of the ith block, the patch type, and the total number of patch types, respectively.

SHAPE_B, and SIDI_B). As shown in Table 2, these 12 distinct feature metrics were employed as independent variables to explain the relationship between these metrics and the cooling intensity of UGS.

3.6. Boosted regression tree

Boosted regression tree (BRT) is a machine learning model that combines the strengths of regression tree with the gradient boosting algorithm (Elith et al., 2008). By utilizing stochastic sampling, adaptive optimization, and iterative refinement, BRT improves model performance and creates a high-efficient, low-error predictive model. It accurately evaluates the relative importance of independent variables and effectively captures the nonlinear relationships between independent and dependent variables (Elith et al., 2008). Consequently, BRT provides reliable and stable predictive performance, even in the presence of complex data and uncertainty. This approach is widely adopted and recognized as an effective machine learning technique.

In this study, 12 metrics (CA UGS, PLAND UGS, PD UGS, LPI UGS, ED_UGS, SHAPE_MN_UGS, AI_UGS, NDVI_UGS, TA_B, PD_B, SHAPE_B, and SIDI_B) were utilized as independent variables, while the diurnal UGS cooling intensities of the four city blocks served as the dependent variables. Initially, Statistical Product and Service Solutions (SPSS) was employed to assess collinearity among the independent variables using the variance inflation factor (VIF) test. Independent variables with VIF values exceeding 10 were excluded (Dewan et al., 2021; Gu and You, 2022). Subsequently, BRT was utilized to analyze the relationship between UGS cooling intensity and the selected independent variables at the city block scale, aiming to determine their relative importance and generate marginal effect maps. The study established the learning rate, tree complexity, and bagging fraction at 0.001, 5, and 0.75, respectively (Han et al., 2024). Additionally, 70 % of the data was allocated for model training, and a 10-fold cross-validation approach was implemented to identify the optimal model (Zhao et al., 2024).

4. Results

4.1. Land cover patterns, diurnal LST variation, and UGS cooling intensity across cities

Fig. 4 shows the land cover classification results for four cities: Beijing, Shanghai, Haikou, and Urumqi. The UGS in Beijing comprised 43.64 %, while Shanghai's UGS accounted for 39.60 %, Haikou's UGS accounted for 37.63 %, and Urumqi's UGS accounted for 18.69 %. The arid climate in Urumqi likely contributed to a notably lower proportion of UGS compared to other cities.

Table 3 presents the classification accuracy for these cities, with an overall accuracy exceeding 93 %.

Fig. 5 illustrates the spatial distribution of diurnal LSTs across the four cities, highlighting significant spatial heterogeneity. During day-time observations, LSTs in these cities were predominantly higher over impervious surfaces. These surfaces, which include buildings and roads, exhibit low albedo and a high capacity for heat absorption, allowing them to rapidly absorb heat. This process significantly enhances the sensible heat flux at the surface, leading to swift localized increases in temperature (Ferrari et al., 2020; Wang et al., 2021). In contrast, the LSTs of water bodies and UGS region were relatively low, with a gradual increase in temperature observed from the edges of the water bodies and UGS outward. Similar to daytime conditions, the temperature of impervious surfaces remained elevated at night. The heat absorbed and stored by these surfaces during the day is slowly dissipated, resulting in persistently high LSTs (Qian et al., 2024).

In contrast to daytime conditions, water bodies exhibited elevated temperatures at night due to their high heat capacity and slow thermal response, resulting in a slight diurnal temperature difference (Yao et al., 2023). While water bodies effectively mitigated the daytime UHI effect, they may not alleviate the nighttime UHI effect due to their inherent characteristics. Conversely, UGS, with its moist soil and vegetative

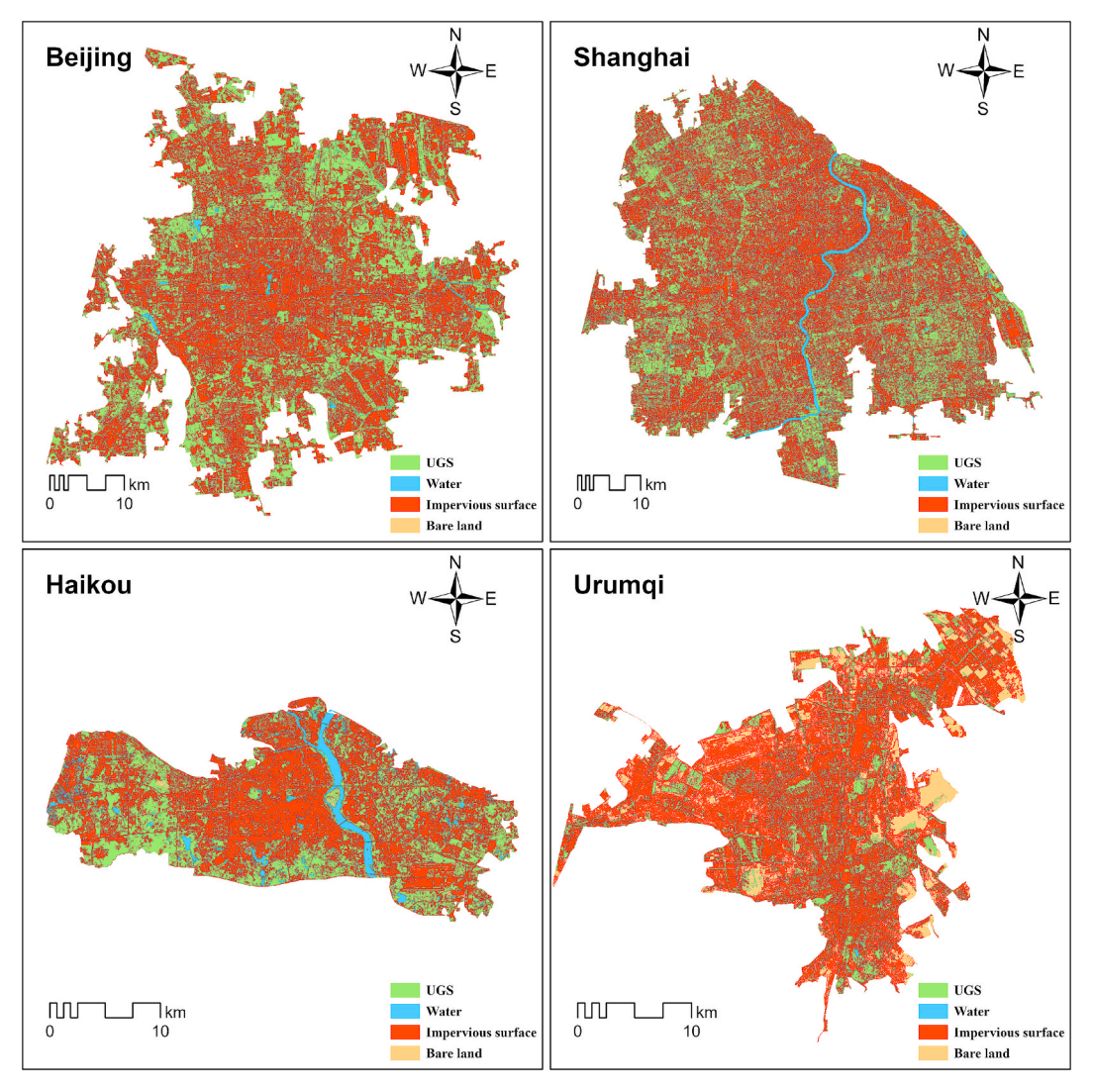


Fig. 4. Spatial distribution of land cover in four cities.

Table 3Accuracy of land cover classification.

City	Beijing	Shanghai	Haikou	Urumqi
Overall Accuracy	93.00 %	93.30 %	94.30 %	93.70 %

cover, mitigated heat accumulation and helped maintain lower nighttime LSTs. It was evident that the diurnal variation of LST differed significantly across the various land cover types in the four cities, and the UGS contributed to mitigating the diurnal UHI effect in all four locations.

Table 4 illustrates that UGS generally exhibit stronger cooling effects during daytime than nighttime, with substantial variation observed across different climate zones. During the daytime, Beijing, Shanghai, and Urumqi exhibited similarly high average cooling intensities, all exceeding 1.1 $^{\circ}$ C, while Haikou demonstrated a noticeably weaker effect. By contrast, nighttime cooling intensities were more uniform across the four cities, ranging narrowly from 0.15 $^{\circ}$ C to 0.20 $^{\circ}$ C, with Haikou exhibiting a slightly stronger intensity than the others.

4.2. Relative importance of urban feature metrics on cooling intensity

Fig. 6 illustrates the relative importance of the 12 feature metrics on daytime UGS cooling intensity across the four cities. Notably, the key

metrics and the extent of their contributions varied among the cities.

The analysis focused on the top three metrics to emphasize the significance of these key metrics. During the daytime, Beijing's leading impact metrics were CA_UGS, ED_UGS, and PD_B, which accounted for 38.97 %, 27.71 %, and 10.06 %, respectively, totaling 76.74 %. Among all the metrics, the UGS landscape metrics and urban block morphology metrics represented 83.39 % and 16.61 %, respectively. In Shanghai, the top three impact metrics were PD B, ED UGS, and CA UGS, contributing 23.88 %, 19.71 %, and 18.44 %, respectively, for a total of 62.03 %. Across all metrics, the UGS landscape metrics, urban block morphology metrics, and UGS biophysical metric accounted for 65.24 %, 29.29 %, and 5.47 %, respectively. For Haikou were TA_B, AI_UGS, and ED_UGS, which accounted for 29.60 %, 26.06 %, and 11.60 %, respectively, totaling 67.26 %. Among all metrics, UGS landscape metrics and urban block morphology metrics represented 58.85 % and 41.15 %, respectively. In Urumqi, the top three key impact metrics were AI_UGS, ED_UGS, and TA_B, accounting for 26.40 %, 20.65 %, and 11.94 %, respectively, totaling 58.99 %. Among all metrics, UGS landscape metrics, urban block morphology metrics, and the UGS biophysical metric accounted for 70.38 %, 21.80 %, and 7.82 %, respectively. It was observed that ED_UGS ranked among the top three metrics in all four cities, while CA_UGS and PD_B ranked among the top three metrics in both Beijing and Shanghai. Additionally, AI_UGS and TA_B ranked among the top three metrics in both Haikou and Urumqi, with AI_UGS

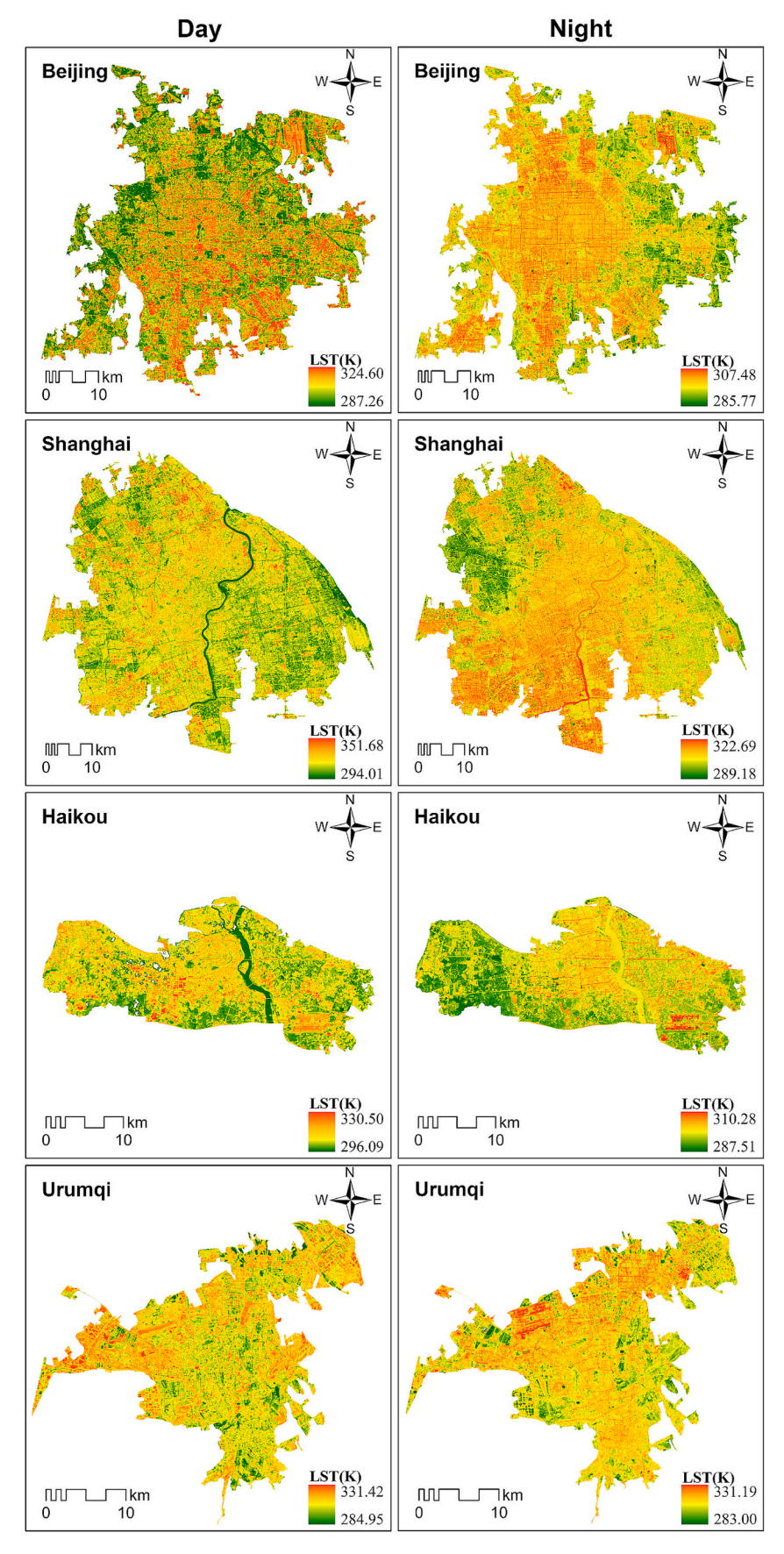


Fig. 5. Spatial patterns of the diurnal LST in four cities.

Table 4Average cooling intensity of UGS in four cities.

City	Average cooling	cooling intensity (°C)	
	Day	Night	
Beijing	1.14	0.16	
Shanghai	1.18	0.15	
Haikou	0.78	0.20	
Urumqi	1.26	0.18	

contributing significantly.

Fig. 7 presents the relative importance of the 12 feature metrics across four cities concerning the nighttime cooling intensity of UGS. During nighttime, the top three key impact metrics for Beijing were AI_UGS, SIDI_B, and CA_UGS, which accounted for 65.33 %, 7.14 %, and 6.28 %, respectively, totaling 78.75 %. Among all metrics, UGS landscape metrics and urban block morphology metrics contributed 86.85 % and 13.15 %, respectively. In Shanghai, the leading three impact metrics were AI_UGS, PD_B, and ED_UGS, which accounted for 56.07 %, 14.87 %, and 10.28 %, respectively, totaling 81.22 %. Here, UGS landscape metrics, urban block morphology metrics, and the UGS biophysical metric represented 79.56 %, 15.96 %, and 4.48 %, respectively. For Haikou, the top three key impact metrics were AI UGS, CA UGS, and ED UGS, which accounted for 44.52 %, 11.95 %, and 9.55 %, respectively, totaling 66.02 %. Among all the metrics, UGS landscape metrics and urban block morphology metrics represented 80.62 % and 19.38 %, respectively. For Urumqi, the top three key impact metrics were AI UGS, PD B, and ED UGS, which accounted for 21.84 %, 12.00 %, and 10.72 %, respectively, totaling 44.56 %. Across all metrics, UGS landscape metrics, urban block morphology metrics, and the UGS biophysical metric accounted for 60.29 %, 32.19 %, and 7.52 %, respectively. Notably, AI_UGS ranked first among the four cities and significant surpassed other metrics in both Beijing and Shanghai.

4.3. Marginal effect of key urban feature metrics on cooling intensity

The top three key metrics regarding the relative contributions of the

four cities to UGS cooling intensity were selected to assess their marginal effects. Fig. 8 illustrates the marginal effects of these key metrics on daytime UGS cooling intensity. During the day, CA_UGS was predominantly positively correlated with UGS cooling intensity, demonstrating a strong positive correlation within the range of $0 \sim 92.90$ ha in Beijing and 0 ~ 134.68 ha in Shanghai. Conversely, ED_UGS exhibited a predominantly negative correlation with UGS cooling intensity, showing a strong negative correlation in Beijing within the range of 19.06 \sim 485.92 m/ha, in Shanghai within the range of 332.27 \sim 681.22 m/ha, Haikou within the range of 26.25 \sim 472.17 m/ha, and in Urumqi within the range of 71.70 ~ 615.04 m/ha. PD_B displayed a monotonic negative correlation with UGS cooling intensity, indicating a strong negative correlation in Beijing within the range of $43.93 \sim 325.98/100$ ha and in Shanghai within the range of $147.43 \sim 573.24/100$ ha. TA B showed a predominant positive correlation with UGS cooling intensity, revealing a strong positive correlation in Haikou within the range of $11.51 \sim 47.40$ ha and in Urumqi within the ranges of 2.51 \sim 88.22 ha and 184.02 \sim 199.15 ha. AI UGS exhibited a predominant positive correlation with UGS cooling intensity, with Haikou showing a strong positive correlation within 94.09 \sim 97.82 % and Urumqi within the range of 88.89 \sim 98.99 %.

Fig. 9 illustrates the marginal effects of key metrics on the intensity of nighttime UGS cooling. During the night, AI_UGS was predominantly positively correlated with UGS cooling intensity, demonstrating a strong positive correlation in Beijing within the range of 82.27 \sim 100 %, in Shanghai within the range of 92.33 ~ 99.33 %, Haikou within the range of 90.68 \sim 96.89 %, and in Urumqi within the range of 88.89 \sim 98.99 %. SIDI_B exhibited a predominant positive correlation with UGS cooling intensity, with Beijing showing a strong positive correlation within the range of 0.05 ~ 0.54. CA_UGS exhibited a predominant positive correlation with UGS cooling intensity, with Beijing within the range of 0 \sim 144.51 ha and Haikou within the range of $0 \sim 11.71$ ha, showing a strong positive correlation with cooling intensity. PD_B exhibited a predominant positive correlation with UGS cooling intensity, with Shanghai showing a strong positive correlation within 147.43 ~ 244.20/100 ha and Urumqi within the 116.03 \sim 263.72/100 ha range. Additionally, Shanghai's nighttime PDB exhibited an inverse

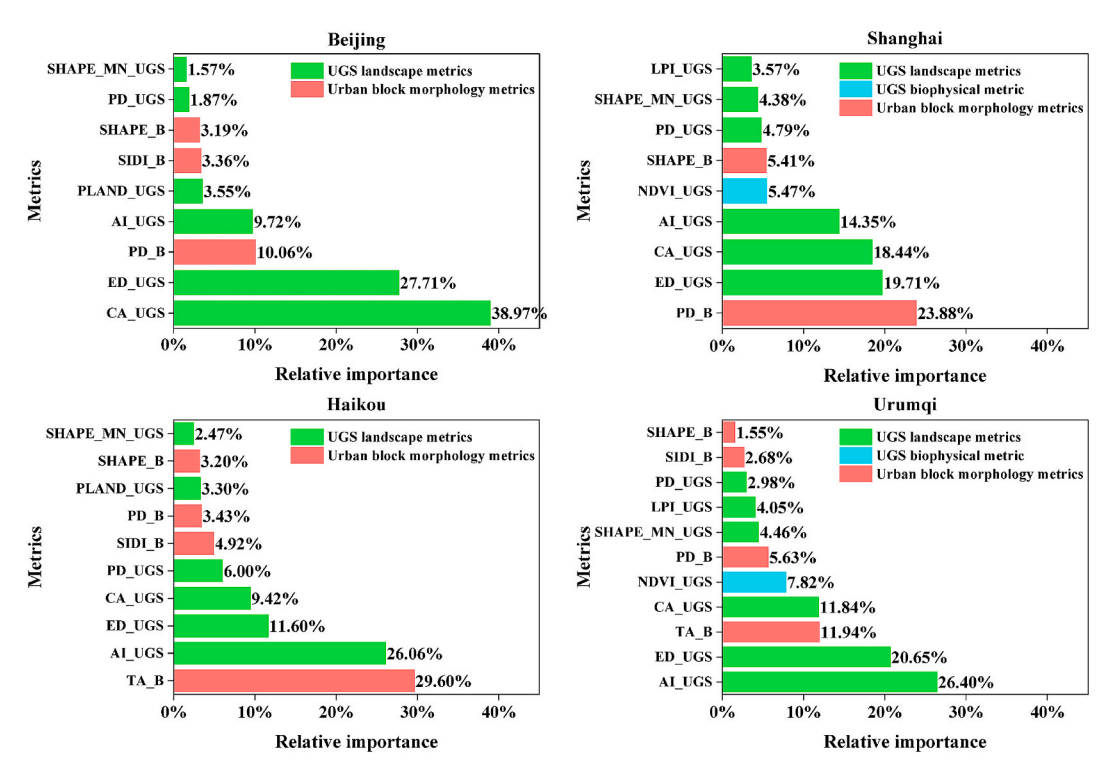


Fig. 6. Relative importance of urban feature metrics in four cities for daytime cooling intensity.

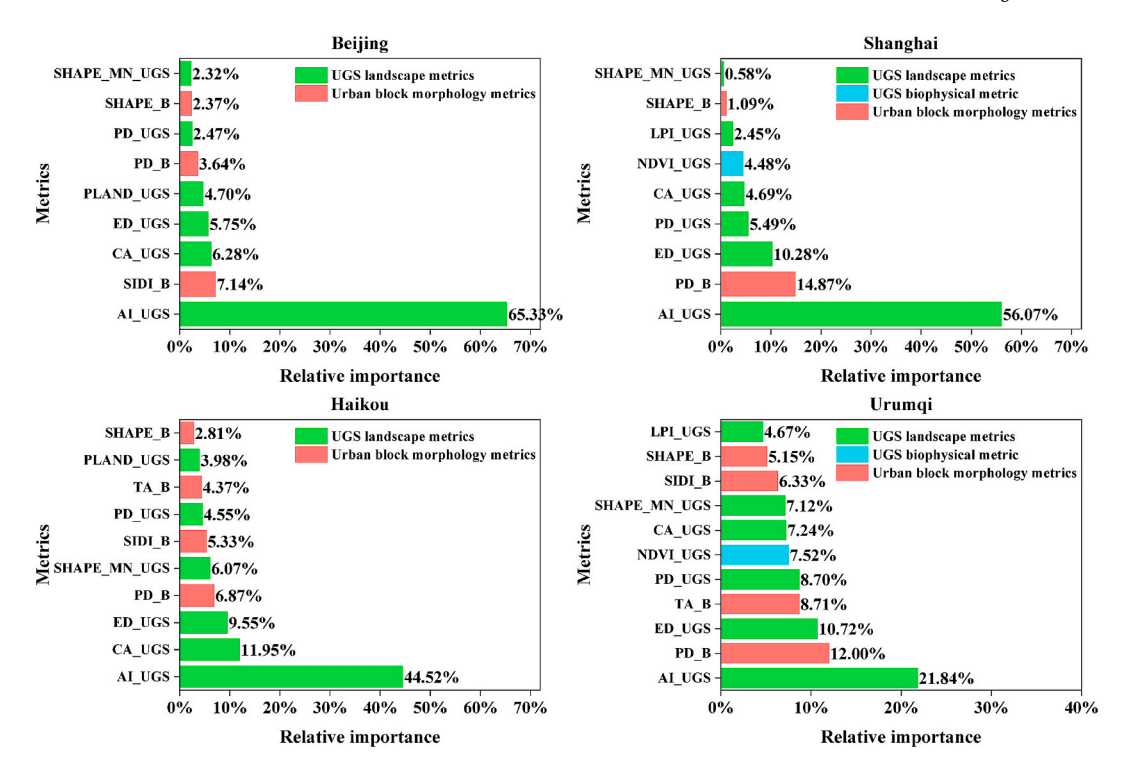


Fig. 7. Relative importance of urban feature metrics in four cities for nighttime cooling intensity.

correlation compared to its daytime correlation. Regarding ED_UGS, Shanghai exhibited a strong negative correlation with cooling intensity within 88 \sim 140.34 m/ha and 166.52 \sim 236.31 m/ha. In contrast, Haikou exhibited a strong positive correlation with cooling intensity within 30.94 \sim 199.01 m/ha and a strong negative correlation within the 199.01 \sim 451.11 m/ha ranges. Urumqi exhibited a strong positive correlation with cooling intensity within the ranges of 0.45 \sim 36.08 m/ha and 160.78 \sim 392.36 m/ha. This indicated that ED_UGS was more sensitive under different climatic background diurnal conditions.

5. Discussion

5.1. Influence of key urban feature metrics on cooling intensity

The study identified significant differences in the cooling effects of UGS across four cities under varying climatic conditions, as evidenced by variations in key metrics and their relative importance. Nevertheless, the cities still exhibit some correlation with one another. During the day, the relative impact levels on the key metrics differ between Beijing and Shanghai; however, the key metrics remain consistent, including CA UGS, ED UGS, and PD B. This consistency may be attributed to the similar biophysical and climatic conditions in both cities—such as hot, humid summers and strong UHI effects—which may produce comparable patterns in UGS cooling performance and landscape configuration. It has been observed that the total area and edge density of UGS significantly influence its cooling effect (Asgarian et al., 2015; Masoudi and Tan, 2019; Yuan et al., 2021). This study further demonstrates that to enhance the cooling intensity of UGS in Beijing and Shanghai, it is essential to improve heat exchange efficiency by strategically planning the total area of UGS, optimizing the complexity of UGS edges, and refining the spatial distribution of block patches. These measures will enhance the microclimatic regulation functions of UGS. Haikou and Urumqi exhibit a similar pattern. Although the relative importance of the three key metrics-TA_B, AI_UGS, and ED_UGS-varies, they consistently rank among the top three contributors. This consistency may stem from the shared characteristics of Haikou and Urumqi, where high-density built-up areas and comparable thermal environments may

produce similar UGS cooling responses through their interaction with UGS spatial configurations. Previous studies have indicated a strong correlation between UGS aggregation and the cold island effect (Zhao et al., 2020). This study suggests that to enhance the cooling intensity of UGS, Haikou and Urumqi should focus on optimizing block size, UGS aggregation levels, and edge density.

Furthermore, the analysis of the nighttime cooling effect reveals that the impact of AI_UGS is particularly pronounced in the four cities, with its magnitude in Beijing and Shanghai significantly exceeding that of the other metrics. This finding underscores the critical role of the UGS aggregation index in determining cooling intensity across various climatic conditions. Therefore, focusing on AI_UGS, or the aggregation index of UGS, will serve as an effective strategy for enhancing the nighttime cooling effect of UGS during the planning and optimization process.

As demonstrated in the marginal effect figures, the changes in UGS cooling intensity due to variations in key feature metric units during the daytime are significantly more pronounced than those observed at night across all four cities, each with distinct climatic conditions. This phenomenon can be attributed to the physiological characteristics of UGS, particularly the closing or narrowing of leaf stomata, which reduces transpiration and subsequently diminishes their cooling effect on LST (Cheung et al., 2024; De Dios et al., 2015). These findings are consistent with the results presented in Table 4, which further underscore the greater cooling effect of UGS during the daytime compared to nighttime. Furthermore, the marginal effects of key metrics reveal distinct optimal values or thresholds that vary significantly across different cities, as shown in Table 5. During the daytime, the optimal values of CA_UGS within the urban blocks of Beijing and Shanghai are 92.90 ha and 134.68 ha, respectively. The optimal values of TA B within the blocks of Haikou and Urumqi are 47.40 ha and 199.15 ha, respectively. When these optimal values are exceeded, the intensity of UGS cooling remains constant despite an increase in UGS area. The thresholds of ED_UGS within the urban blocks of Beijing, Shanghai, Haikou, and Urumqi are 19.06 m/ha, 332.27 m/ha, 26.25 m/ha, and 71.70 m/ha, respectively. When these thresholds are surpassed, the intensity of UGS cooling decreases as the density of the UGS edge increases. The thresholds of PD B within the blocks of Beijing and Shanghai are 43.93/100 ha and 147.43/

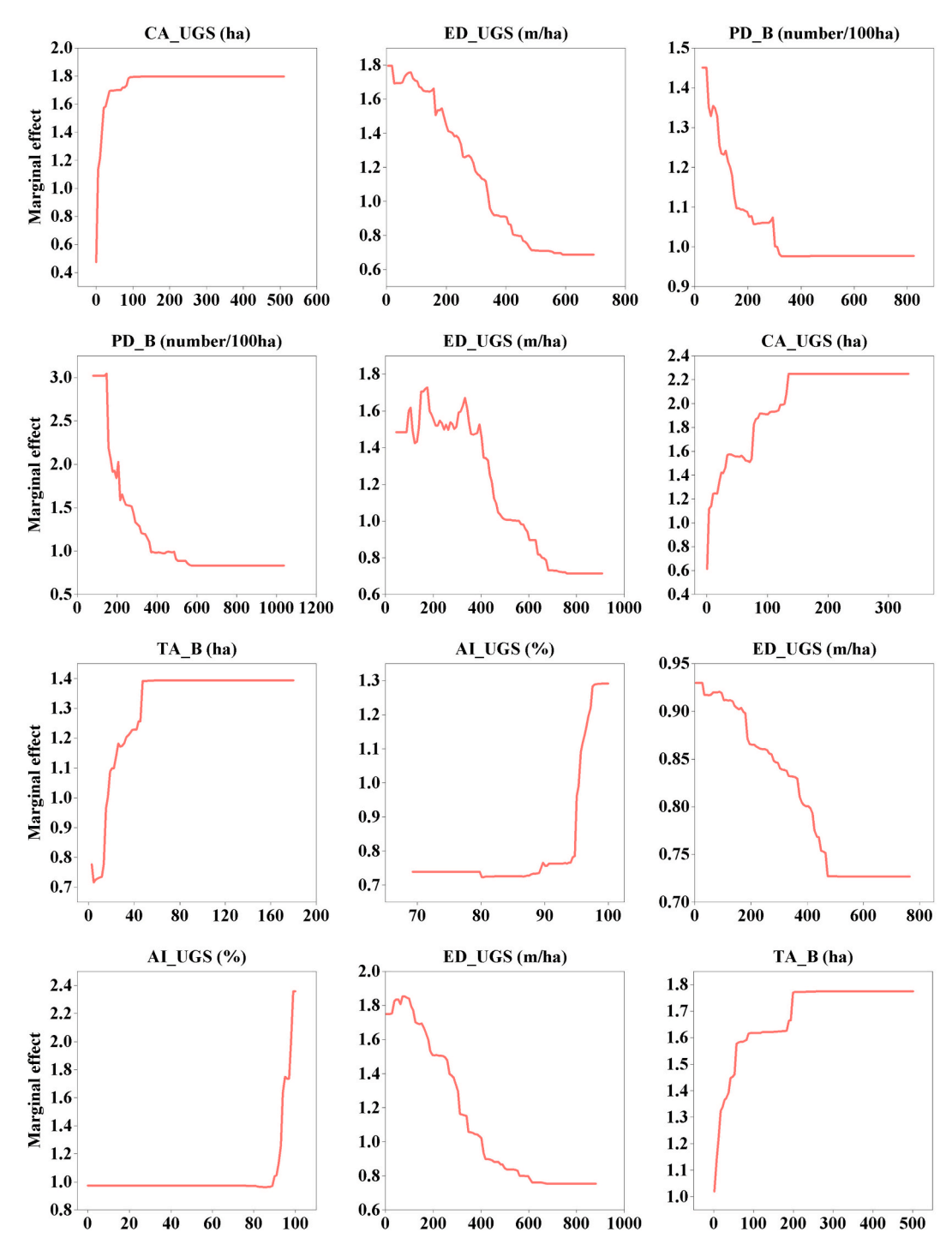


Fig. 8. Marginal effect of key urban feature metrics on daytime cooling intensity in four cities.

100 ha, respectively. When these thresholds are exceeded, the intensity of UGS cooling decreases as block patch density increases. The thresholds of AI_UGS within the blocks of Haikou and Urumqi are 94.09 % and 88.89 %, respectively. When these thresholds are surpassed, the cooling intensity of UGS increases with the UGS aggregation index. At night, the optimal value of SIDI_B in the Beijing blocks is 0.54. The optimal values of CA_UGS in the Beijing and Haikou blocks are 144.51 ha and 11.71 ha, respectively. Similarly, the optimal values of PD_B in the Shanghai and Urumqi blocks are 244.20/100 ha and 263.72/100 ha, respectively, while the optimal value of ED_UGS in the Urumqi blocks is 392.36 m/ha. Once these optimal values are exceeded, the UGS cooling intensity remains unchanged despite further increases in the index values. The

optimal value of ED_UGS within the Haikou blocks is 199.01 m/ha. Once this threshold is exceeded, the intensity of UGS cooling declines as the density of the UGS edge increases. The thresholds of AI_UGS within the urban blocks of Beijing, Shanghai, Haikou, and Urumqi are 82.27 %, 92.33 %, 90.68 %, and 88.89 %, respectively. When these thresholds are exceeded, the intensity of UGS cooling increases in proportion to the index of UGS aggregation. The threshold value of ED_UGS within urban blocks in Shanghai is 88 m/ha. Once this threshold is surpassed, the intensity of UGS cooling declines as the density of UGS edges increases.

This study presents targeted urban block UGS planning recommendations for cities with varying climate types to optimize UGS cooling intensity. In cities characterized by warm temperate monsoon climates

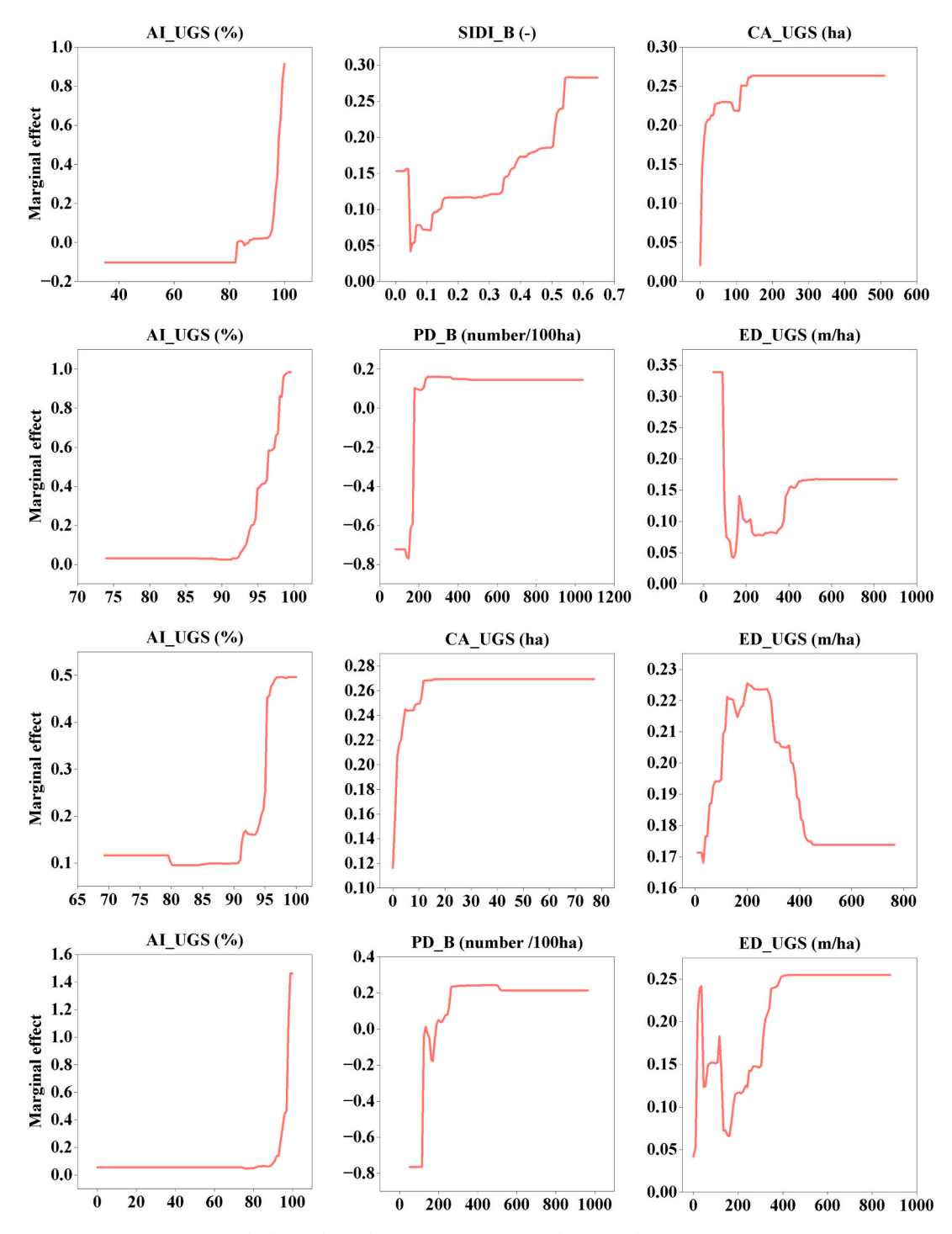


Fig. 9. Marginal effect of key urban feature metrics on nighttime cooling intensity in four cities.

(e.g., Beijing) and subtropical monsoon climates (e.g., Shanghai), it is advisable to moderately increase the total UGS area within city blocks (Beijing: < 92.90 ha; Shanghai: < 134.68 ha). These recommendations are grounded in research findings that identify optimal UGS configurations for maximizing cooling effects. This expansion can be achieved through vertical greening techniques that do not require additional land. Additionally, UGS should be designed in regular shapes (e.g., circular or square) to maximize cooling benefits (Feyisa et al., 2014; Cao et al., 2010). Furthermore, fragmented UGS should be integrated, block patch density should be reduced, and the spatial aggregation of UGS should be improved by connecting fragmented UGS patches through green space corridors or ecological buffer zones, as demonstrated in Beijing (82.27)

%) and Shanghai (92.33 %). These strategies effectively enhance the cooling effect of UGS during both daytime and nighttime periods. These strategies can support evidence-based urban planning practices aimed at mitigating thermal risks and improving outdoor thermal comfort.

For tropical monsoon cities (e.g., Haikou) and cities with midtemperate arid climates (e.g., Urumqi), urban planning should appropriately expand the total area of blocks (Haikou: < 47.40 ha; Urumqi: < 199.15 ha) and optimize the building layout to create ventilation corridors that facilitate heat dissipation within these blocks. Additionally, fragmented UGS patches should be consolidated, and UGS aggregation areas should be centrally planned, with supplementary horizontal and vertical greening measures implemented to enhance UGS aggregation

Table 5Optimal value or thresholds of key metrics for UGS cooling intensity.

City	Day Optimal value	Threshold value	Night Optimal value	Threshold value
Beijing	CA_UGS (92.90 ha)	ED_UGS (19.06 m/ha) PD_B (43.93/ 100 ha)	SIDI_B (0.54) CA_UGS (144.51 ha)	AI_UGS (82.27 %)
Shanghai	CA_UGS (134.68 ha)	ED_UGS (332.27 m/ha) PD_B (147.43/ 100 ha)	PD_B (244.20/ 100 ha)	AI_UGS (92.33 %) ED_UGS (88 m/ha)
Haikou	TA_B (47.40 ha)	ED_UGS (26.25 m/ha) AI_UGS (94.09 %)	CA_UGS (11.71 ha) ED_UGS (199.01 m/ha)	AI_UGS (90.68 %)
Urumqi	TA_B (199.15 ha)	ED_UGS (71.70 m/ha) AI_UGS (88.89 %)	PD_B (263.72/ 100 ha) ED_UGS (392.36 m/ha)	AI_UGS (88.89 %)

(Haikou: > 90.68 %; Urumqi: > 88.89 %). This study offers quantitative references through its findings to inform localized urban planning and UGS-related regulations. In tropical monsoon cities like Haikou, the coverage and aggregation effect of UGS can be improved by increasing the total UGS area (Haikou: < 11.71 ha) through the development of micro-parks on abandoned land and underutilized spaces. In contrast, for arid cities in the mid-temperate zone, such as Urumqi, increasing block patch density by subdividing large UGSs into smaller ones and decentralizing their layout (Urumqi: < 263.72/100 ha) can enhance the nighttime cooling function of UGS. In future research, these recommendations could be further validated through case-based applications in collaboration with urban planning agencies, enhancing their relevance for real-world governance.

5.2. Limitations

This study has several limitations. First, while it examines the intensity of diurnal UGS cooling in four typical urban blocks with varying climatic backgrounds, it does not include data from other cities with similar climatic conditions, which may limit the generalizability of the findings. Future research should incorporate a broader range of cities to enhance the robustness of the results. Second, conducting comparative studies that collect diurnal LSTs on the same day to obtain more precise measurements of diurnal UGS cooling effects presents methodological challenges. Third, as this study focuses primarily on the summer season, its conclusions may not be applicable across different seasons. Future research should explore seasonal variations in UGS cooling intensity. Fourth, future research should integrate three-dimensional (3D) features, such as building height and volume, for a more comprehensive understanding of how urban block structure affects UGS cooling. Finally, the functional types of blocks (e.g., residential, commercial, industrial) were not considered in this study. Future work should incorporate these attributes, along with broader factors such as urban planning, infrastructure development, and environmental policies, to better understand the drivers of spatial variation in UGS cooling effects.

6. Conclusions

This study analyzed the influence of block-scale UGS landscape metrics, a UGS biophysical metric, and urban block morphology metrics on the diurnal cooling intensity of UGS in four representative cities: Beijing, Shanghai, Haikou, and Urumqi. The analysis was conducted under varying climatic conditions using SDGSAT-1/TIS data and GF multispectral imagery. Employing the boosted regression tree algorithm, we examined the diurnal temperature differences among various land cover types and explored the relative importance and marginal

effects of key feature metrics. The results of the study indicated that: (1) During the day, LSTs in the four cities were generally higher in areas with impervious surfaces compared to water bodies and UGS areas. At night, LSTs were higher in the impervious surfaces and water bodies, while they were lower in UGS areas. UGS maintained a relatively low LST both during the day and at night, with its cooling effect being more pronounced during the day than at night. (2) The key metrics for daytime UGS cooling intensity varied across the four cities under different climatic conditions. The relative importance of these metrics and their correlations were as follows: Beijing (CA_UGS: 38.97 %, +; ED_UGS: 27.71 %, -; PD_B: 10.06 %, -); Shanghai (PD_B: 23.88 %, -; ED_UGS: 19.71 %, –; CA_UGS: 18.44 %, +); Haikou (TA_B: 29.60 %, +; AI_UGS: 26.06 %, +; ED_UGS: 11.60 %, -); Urumqi (AI_UGS: 26.40 %, +; ED_UGS: 20.65 %, -; TA_B: 11.94 %, +). Beijing and Shanghai shared the same key metrics, demonstrating a consistent correlation between these metrics and UGS cooling intensity. A similar relationship was observed for Haikou and Urumqi. At night, AI_UGS emerged as the most significant metric in all four cities, with positive correlations observed in Beijing (65.33 %), Shanghai (56.07 %), Haikou (44.52 %), and Urumqi (21.84 %). (3) The key urban metrics exhibited a non-linear relationship with cooling intensity across different climatic contexts. By analyzing the marginal effects, the optimal or threshold value of each key metric was determined, revealing significant differences among the cities. This study provides important theoretical insights and practical guidance for optimizing UGS landscapes in diverse climatic contexts.

CRediT authorship contribution statement

Chang Liu: Writing – original draft, Visualization, Methodology, Formal analysis, Conceptualization. Xiaoying Ouyang: Writing – review & editing. Jinxin Yang: Writing – review & editing. Dinoo Gunasekera: Writing – review & editing. Qihao Weng: Writing – review & editing. Xuesheng Zhao: Writing – review & editing. Zhongchang Sun: Supervision, Funding acquisition.

Declaration of competing interest

The authors declare that they have no known competing financial interests or personal relationships that could have appeared to influence the work reported in this paper.

Acknowledgments

This work was supported by the National Natural Science Foundation of China (Grant No. 42471363, 42361144884, 42171370), and the Joint HKU-CAS Laboratory for iEarth (313GJHZ2022074MI, E4F3050300).

Appendix A. Supplementary data

Supplementary data to this article can be found online at https://doi.org/10.1016/j.ecolind.2025.113937.

Data availability

Data will be made available on request.

References

Arellano, B., Roca, J., 2021. Remote sensing and night time urban heat island. Int. Arch. Photogramm. Remote. Sens. Spat. Inf. Sci. 43, 15–22. https://doi.org/10.5194/isprs-archives-XLIII-B3-2021-15-2021.

Asgarian, A., Amiri, B.J., Sakieh, Y., 2015. Assessing the effect of green cover spatial patterns on urban land surface temperature using landscape metrics approach. Urban Ecosystems. 18, 209–222. https://doi.org/10.1007/s11252-014-0387-7.

Athokpam, V., Chamroy, T., Ngairangbam, H., 2024. The role of urban green spaces in mitigating climate change: an integrative review of ecological, social, and health benefits. Environmental reports; an. Int. J. 10–14. https://doi.org/10.51470/ER.2024.6.1.10.

- Bai, Y., Wang, K., Ren, Y., Li, M., Ji, R., Wu, X., Yan, H., Lin, T., Zhang, G., Zhou, X., 2024. 3D compact form as the key role in the cooling effect of greenspace landscape pattern. Ecol. Ind. 160, 111776. https://doi.org/10.1016/j.ecolind.2024.111776.
- Bakhshoodeh, R., Ocampo, C., Oldham, C., 2022. Evapotranspiration rates and evapotranspirative cooling of green façades under different irrigation scenarios. Energ. Buildings 270, 112223. https://doi.org/10.1016/j.enbuild.2022.112223.
- Barriopedro, D., García-Herrera, R., Ordóñez, C., Miralles, D., Salcedo-Sanz, S., 2023. Heat waves: Physical understanding and scientific challenges. Rev. Geophys. 61, e2022RG000780. https://doi.org/10.1029/2022RG000780.
- Beijing Municipal Bureau Statistics, 2023. Beijing statistical yearbook 2023. Retrieved from https://nj.tjj.beijing.gov.cn/nj/main/2023-tjnj/zk/indexch.htm (in Chinese). Accessed September 6, 2024.
- Cao, X., Onishi, A., Chen, J., Imura, H., 2010. Quantifying the cool island intensity of urban parks using ASTER and IKONOS data. Landsc. Urban Plan. 96, 224–231. https://doi.org/10.1016/j.landurbplan.2010.03.008.
- Chen, Y., Yang, J., Yu, W., Ren, J., Xiao, X., Xia, J.C., 2023. Relationship between urban spatial form and seasonal land surface temperature under different grid scales. Sustain. Cities Soc. 89, 104374. https://doi.org/10.1016/j.scs.2022.104374.
- Chen, Y.-C., Hou, K.-S., Liao, Y.-J., Honjo, T., Cheng, F.-Y., Lin, T.-P., 2024. The application of a high-density street-level air temperature observation network (HiSAN): Spatial and temporal variations of thermal and wind condition in different climatic condition types. Sustain. Cities Soc. 109, 105547. https://doi.org/10.1016/j.scs.2024.105547.
- Cheung, P.K., Livesley, S.J., Nice, K.A., 2021. Estimating the cooling potential of irrigating green spaces in 100 global cities with arid, temperate or continental climates. Sustain. Cities Soc. 71, 102974. https://doi.org/10.1016/j. scs.2021.102974.
- Cheung, P.K., Meili, N., Nice, K.A., Livesley, S.J., 2024. Identifying the mechanisms by which irrigation can cool urban green spaces in summer. Urban Clim. 55, 101914. https://doi.org/10.1016/j.uclim.2024.101914.
- Cui, P., Xv, D., Tang, J., Lu, J., Wu, Y., 2024. Assessing the effects of urban green spaces metrics and spatial structure on LST and carbon sinks in Harbin, a cold region city in China. Sustain. Cities Soc. 113, 105659. https://doi.org/10.1016/j. scs.2024.105659.
- De Dios, V.R., Roy, J., Ferrio, J.P., Alday, J.G., Landais, D., Milcu, A., Gessler, A., 2015. Processes driving nocturnal transpiration and implications for estimating land evapotranspiration. Sci. Rep. 5, 10975. https://doi.org/10.1038/srep10975.
- Dewan, A., Kiselev, G., Botje, D., Mahmud, G.I., Bhuian, M.H., Hassan, Q.K., 2021. Surface urban heat island intensity in five major cities of Bangladesh: patterns, drivers and trends. Sustain. Cities Soc. 71, 102926. https://doi.org/10.1016/j.scs.2021.102926.
- Dong, J., Guo, R., Lin, M., Guo, F., Zheng, X., 2024. Multi-objective optimization of green roof spatial layout in high-density urban areas—A case study of Xiamen Island, China. Sustainable Cities and Society 115, 105827. https://doi.org/10.1016/j. sec.2024.105827.
- Dong, Y., Ren, Z., Fu, Y., Hu, N., Guo, Y., Jia, G., He, X., 2022. Decrease in the residents' accessibility of summer cooling services due to green space loss in chinese cities. Environ. Int. 158, 107002. https://doi.org/10.1016/j.envint.2021.107002.
- Elith, J., Leathwick, J.R., Hastie, T., 2008. A working guide to boosted regression trees. J. Anim. Ecol. 77, 802–813. https://doi.org/10.1111/j.1365-2656.2008.01390.x.
- Esperon-Rodriguez, M., Tjoelker, M.G., Lenoir, J., Baumgartner, J.B., Beaumont, L.J., Nipperess, D.A., Power, S.A., Richard, B., Rymer, P.D., Gallagher, R.V., 2022. Climate change increases global risk to urban forests. Nat. Clim. Chang. 12, 950–955. https://doi.org/10.1038/s41558-022-01465-8.
- Ferrari, A., Kubilay, A., Derome, D., Carmeliet, J., 2020. The use of permeable and reflective pavements as a potential strategy for urban heat island mitigation. Urban Clim. 31, 100534. https://doi.org/10.1016/j.uclim.2019.100534.
- Feyisa, G.L., Dons, K., Meilby, H., 2014. Efficiency of parks in mitigating urban heat island effect: an example from Addis Ababa. Landsc. Urban Plan. 123, 87–95. https://doi.org/10.1016/j.landurbplan.2013.12.008.
- Gu, Y., You, X.-Y., 2022. A spatial quantile regression model for driving mechanism of urban heat island by considering the spatial dependence and heterogeneity: an example of Beijing, China. Sustainable Cities and Society. 79, 103692. https://doi. org/10.1016/j.scs.2022.103692.
- Guha, S., Govil, H., 2021. An assessment on the relationship between land surface temperature and normalized difference vegetation index. Environ. Dev. Sustain. 23, 1944–1963. https://doi.org/10.1007/s10668-020-00657-6.
- Guo, A., Yue, W., Yang, J., Li, M., Xie, P., He, T., Zhang, M., Yu, H., 2023a. Quantifying the impact of urban ventilation corridors on thermal environment in chinese megacities. Ecol. Ind. 156, 111072. https://doi.org/10.1016/j. ecolind.2023.111072.
- Guo, H., Dou, C., Chen, H., Liu, J., Fu, B., Li, X., Zou, Z., Liang, D., 2023b. SDGSAT-1: the world's first scientific satellite for sustainable development goals. Sci. Bull. 68, 34–38. https://doi.org/10.1016/j.scib.2022.12.014.
- Guo, H., Liang, D., Sun, Z., Chen, F., Wang, X., Li, J., Zhu, L., Bian, J., Wei, Y., Huang, L., 2022. Measuring and evaluating SDG indicators with big earth data. Science Bulletin. 67, 1792–1801. https://doi.org/10.1016/j.scib.2022.07.015.
- Haikou Municipal Bureau Statistics, 2023. Haikou statistical yearbook 2023. Re-trieved from http://tjj.haikou.gov.cn/hkstjj/tjnj/202312/ 0b6fd7c77da646b08cd97a2e97a8353a.shtml (in Chinese). Accessed September 6, 2024.
- Han, D., An, H., Cai, H., Wang, F., Xu, X., Qiao, Z., Jia, K., Sun, Z., An, Y., 2023. How do 2D/3D urban landscapes impact diurnal land surface temperature: Insights from block scale and machine learning algorithms. Sustain. Cities Soc. 99, 104933. https://doi.org/10.1016/j.scs.2023.104933.

- Han, D., Cai, H., Wang, F., Wang, M., Xu, X., Qiao, Z., An, H., Liu, Y., Jia, K., Sun, Z., 2024. Understanding the role of urban features in land surface temperature at the block scale: a diurnal cycle perspective. Sustain. Cities Soc. 111, 105588. https://doi.org/10.1016/j.scs.2024.105588.
- He, B.-J., Wang, J., Zhu, J., Qi, J., 2022. Beating the urban heat: Situation, background, impacts and the way forward in China. Renew. Sustain. Energy Rev. 161, 112350. https://doi.org/10.1016/j.rser.2022.112350.
- Hu, D., Meng, Q., Schlink, U., Hertel, D., Liu, W., Zhao, M., Guo, F., 2022. How do urban morphological blocks shape spatial patterns of land surface temperature over different seasons? a multifactorial driving analysis of Beijing, China. Int. J. Appl. Earth Obs. Geoinf. 106, 102648. https://doi.org/10.1016/j.jag.2021.102648.
- Huang, B., He, B.-J., 2025. Lawn and irrigation cooling from ground longwave radiation reduction: Understanding the climate-driven variability in cooling performance. Urban Clim. 60, 102360. https://doi.org/10.1016/j.uclim.2025.102360.
- Huang, K., Lee, X., Stone Jr, B., Knievel, J., Bell, M.L., Seto, K.C., 2021. Persistent increases in nighttime heat stress from urban expansion despite heat island mitigation. J. Geophys. Res. Atmos. 126, e2020JD033831. https://doi.org/10.1029/ 2020JD033831.
- Jiang, H., Sun, Z., Guo, H., Weng, Q., Du, W., Xing, Q., Cai, G., 2021. An assessment of urbanization sustainability in China between 1990 and 2015 using land use efficiency indicators. Npj Urban Sustainability. 1, 34. https://doi.org/10.1038/ s42949-021-00032-y.
- Ke, X., Men, H., Zhou, T., Li, Z., Zhu, F., 2021. Variance of the impact of urban green space on the urban heat island effect among different urban functional zones: a case study in Wuhan. Urban For. Urban Green. 62, 127159. https://doi.org/10.1016/j. ufug.2021.127159.
- Khan, M.S., Li, Y., 2024. Comparative study and effects of urban green scape on the land surface temperature of a large metropolis and green city. Heliyon 10. https://doi. org/10.1016/j.heliyon.2024.e24912.
- Li, J., Wu, H., Li, Z.-L., 2020. An optimal sampling method for multi-temporal land surface temperature validation over heterogeneous surfaces. ISPRS J. Photogramm. Remote Sens. 169, 29–43. https://doi.org/10.1016/j.isprsjprs.2020.08.024.
- Li, L., Zhou, X., Hu, Z., Gao, L., Li, X., Ni, X., Chen, F., 2023a. On-orbit monitoring flying aircraft day and night based on SDGSAT-1 thermal infrared dataset. Remote Sens. Environ. 298, 113840. https://doi.org/10.1016/j.rse.2023.113840.
- Li, Y., Li, Z.-L., Wu, H., Zhou, C., Liu, X., Leng, P., Yang, P., Wu, W., Tang, R., Shang, G.-F., 2023b. Biophysical impacts of earth greening can substantially mitigate regional land surface temperature warming. Nat. Commun. 14, 121. https://doi.org/10.1038/sd1467-023-35799-4
- Li, Y., Ren, C., Ho, J.Y.e., Shi, Y., 2023c. Landscape metrics in assessing how the configuration of urban green spaces affects their cooling effect: a systematic review of empirical studies. Landsc. Urban Plan. 239, 104842. https://doi.org/10.1016/j. landurbplan.2023.104842.
- Li, Z.L., Wu, H., Duan, S.B., Zhao, W., Ren, H., Liu, X., Leng, P., Tang, R., Ye, X., Zhu, J., 2023d. Satellite remote sensing of global land surface temperature: Definition, methods, products, and applications. Rev. Geophys. 61. https://doi.org/10.1029/ 2022RG000777.
- Liu, W., Zhang, L., Hu, X., Meng, Q., Qian, J., Gao, J., Li, T., 2024. Nonlinear effects of urban multidimensional characteristics on daytime and nighttime land surface temperature in highly urbanized regions: a case study in Beijing, China. Int. J. Appl. Earth Obs. Geoinf. 132, 104067. https://doi.org/10.1016/j.jag.2024.104067.
- Liu, X., Li, Z.-L., Li, Y., Wu, H., Zhou, C., Si, M., Leng, P., Duan, S.-B., Yang, P., Wu, W., 2023. Local temperature responses to actual land cover changes present significant latitudinal variability and asymmetry. Science Bulletin. 68, 2849–2861. https://doi. org/10.1016/j.scib.2023.09.046.
- Marcotullio, P.J., Keßler, C., Fekete, B.M., 2022. Global urban exposure projections to extreme heatwaves. Front. Built Environ. 8, 947496. https://doi.org/10.3389/fbuil 2022 947496
- Masoudi, M., Tan, P.Y., 2019. Multi-year comparison of the effects of spatial pattern of urban green spaces on urban land surface temperature. Landsc. Urban Plan. 184, 44–58. https://doi.org/10.1016/j.landurbplan.2018.10.023.
- Nasar-u-Minallah, M., Haase, D., Qureshi, S., 2024. Evaluating the impact of landscape configuration, patterns and composition on land surface temperature: an urban heat island study in the Megacity Lahore, Pakistan. Environmental Monitoring and Assessment 196 627 https://doi.org/10.1007/s10661-024-12758-0
- Assessment. 196, 627. https://doi.org/10.1007/s10661-024-12758-0.

 Nie, X., Lin, J., Ma, J., Cao, B., Li, Y., Lu, Y., Bian, Y., Liu, J., Zhang, P., 2024. The cooling effect of plant configuration on urban parks green space in temperate continental climate zones. Appl. Spat. Anal. Policy 17, 1463–1483. https://doi.org/10.1007/s12061-024-09590-x.
- Ouyang, X., Sun, Z., Zhou, S., Dou, Y., 2024. Urban land surface temperature retrieval with high-spatial resolution SDGSAT-1 thermal infrared data. Remote Sens. Environ. 312, 114320. https://doi.org/10.1016/j.rse.2024.114320.
- Peng, H., Lou, H., Yang, Y., He, Q., Liu, Y., Chen, E., Zhang, M., 2025. Spatial and Temporal Heterogeneity of Human-Air-Ground Coupling Relationships at Fine Scale. Pol. J. Environ. Stud. 1–21. https://doi.org/10.15244/pjoes/197055.
- Qian, F., Hu, Y., Wu, R., Yan, H., Wang, D., Xiang, Z., Zhao, K., Han, Q., Shao, F., Bao, Z., 2024. Assessing the spatial-temporal impacts of underlying surfaces on 3D thermal environment: a field study based on UAV vertical measurements. Build. Environ. 265, 111985. https://doi.org/10.1016/j.buildenv.2024.111985.
- Rakoto, P.Y., Deilami, K., Hurley, J., Amati, M., Sun, Q.C., 2021. Revisiting the cooling effects of urban greening: Planning implications of vegetation types and spatial configuration. Urban For. Urban Green. 64, 127266. https://doi.org/10.1016/j. urba.2021.127266
- Ren, J., Yang, J., Wu, F., Sun, W., Xiao, X., Xia, J.C., 2023. Regional thermal environment changes: Integration of satellite data and land use/land cover. iScience 26 (2), 105820. https://doi.org/10.1016/j.isci.2022.105820.

- Ren, J., Yang, J., Yu, W., Cong, N., Xiao, X., Xia, J.C., Li, X., 2024. Investigating the attribution of urban thermal environment changes under background climate and anthropogenic exploitation scenarios. Sustain. Cities Soc. 107, 105466. https://doi. org/10.1016/j.scs.2024.105466.
- Shah, A., Garg, A., Mishra, V., 2021. Quantifying the local cooling effects of urban green spaces: evidence from Bengaluru, India. Landscape and Urban Planning. 209, 104043. https://doi.org/10.1016/j.landurbplan.2021.104043.
- Shanghai Municipal Bureau Statistics, 2023. Shanghai statistical yearbook 2023. Retrieved from https://tjj.sh.gov.cn/tjnj/tjnj2023.htm (in Chinese). Accessed September 6, 2024.
- Shi, D., Song, J., Huang, J., Zhuang, C., Guo, R., Gao, Y., 2020. Synergistic cooling effects (SCEs) of urban green-blue spaces on local thermal environment: a case study in Chongqing. China. Sustainable Cities and Society. 55, 102065. https://doi.org/ 10.1016/j.scs.2020.102065.
- Sun, J., Sun, Z., Guo, H., Wang, J., Jiang, H., Gao, J., 2022. A dataset of built-up areas of chinese cities in 2020, China. Scientific Data. 7. https://doi.org/10.11922/ sciencedb.i00001.00332.
- Sun, R., Wang, Y., Chen, L., 2018. A distributed model for quantifying temporal-spatial patterns of anthropogenic heat based on energy consumption. J. Clean. Prod. 170, 601–609. https://doi.org/10.1016/j.jclepro.2017.09.153.
- Tan, X., Sun, X., Huang, C., Yuan, Y., Hou, D., 2021. Comparison of cooling effect between green space and water body. Sustain. Cities Soc. 67, 102711. https://doi. org/10.1016/j.scs.2021.102711.
- Tehrani, A.A., Veisi, O., Delavar, Y., Bahrami, S., Sobhaninia, S., Mehan, A., 2024.

 Predicting urban Heat Island in European cities: a comparative study of GRU, DNN, and ANN models using urban morphological variables. Urban Clim. 56, 102061. https://doi.org/10.1016/j.uclim.2024.102061.
- Urumqi Municipal Bureau Statistics, 2024. Urumqi statistical yearbook 2023. R-etrieved from https://www.urumqi.gov.cn/wlmqs/c119359/202404/ 2b61a91bdcd2491dbe5756de6d9c90d9.shtml (in Chinese). Accessed September 6, 2024
- Wang, A., Dai, Y., Zhang, M., Chen, E., 2025. Exploring the cooling intensity of green cover on urban heat island: a case study of nine main urban districts in Chongqing. Sustain. Cities Soc. 124, 106299. https://doi.org/10.1016/j.scs.2025.106299.
- Wang, C., Ren, Z., Dong, Y., Zhang, P., Guo, Y., Wang, W., Bao, G., 2022. Efficient cooling of cities at global scale using urban green space to mitigate urban heat island effects in different climatic regions. Urban For. Urban Green. 74, 127635. https://doi.org/10.1016/j.ufug.2022.127635.
- Wang, C., Wang, Z.-H., Kaloush, K.E., Shacat, J., 2021. Cool pavements for urban heat island mitigation: a synthetic review. Renew. Sustain. Energy Rev. 146, 111171. https://doi.org/10.1016/j.rser.2021.111171.
- Wang, Q., Peng, J., Yu, S., Dan, Y., Dong, J., Zhao, X., Wu, J., 2023. Key attributes of greenspace pattern for heat mitigation vary with urban functional zones. Landsc. Ecol. 38, 2965–2979. https://doi.org/10.1007/s10980-023-01763-2.
- Wei, S., He, Z., Zhai, W., Zhao, C., Li, Y., 2025. How does vegetation influence surface temperature across various road types and urban morphology types? Build. Environ. 270, 112511. https://doi.org/10.1016/j.buildenv.2024.112511.

- Yang, C., Zhao, S., 2024. Synergies or trade-offs between surface urban heat island and hot extreme: Distinct responses in urban environments. Sustain. Cities Soc. 101, 105093. https://doi.org/10.1016/j.scs.2023.105093.
- Yang, F., Yousefpour, R., Hu, Y., Zhang, Y., Li, J., Wang, H., 2024. Assessing the efficiency of urban blue-green space in carbon-saving: take a high-density urban area in a cold region as an example. J. Clean. Prod. 479, 144017. https://doi.org/ 10.1016/i.jclepro.2024.144017.
- Yang, J., Shi, Q., Menenti, M., Xie, Y., Wu, Z., Xu, Y., Abbas, S., 2022. Characterizing the thermal effects of vegetation on urban surface temperature. Urban Clim. 44, 101204. https://doi.org/10.1016/j.uclim.2022.101204.
- Yao, L., Li, T., Xu, M., Xu, Y., 2020. How the landscape features of urban green space impact seasonal land surface temperatures at a city-block-scale: an urban heat island study in Beijing, China. Urban Forestry & Urban Greening. 52, 126704. https://doi. org/10.1016/j.ufug.2020.126704.
- Yao, L., Sailor, D.J., Yang, X., Xu, G., Zhao, L., 2023. Are water bodies effective for urban heat mitigation? evidence from field studies of urban lakes in two humid subtropical cities. Build. Environ. 245, 110860. https://doi.org/10.1016/j. buildenv.2023.110860.
- Yu, Z., Chen, J., Chen, J., Zhan, W., Wang, C., Ma, W., Yao, X., Zhou, S., Zhu, K., Sun, R., 2024. Enhanced observations from an optimized soil-canopy-photosynthesis and energy flux model revealed evapotranspiration-shading cooling dynamics of urban vegetation during extreme heat. Remote Sens. Environ. 305, 114098. https://doi.org/10.1016/j.rse.2024.114098.
- Yuan, B., Zhou, L., Dang, X., Sun, D., Hu, F., Mu, H., 2021. Separate and combined effects of 3D building features and urban green space on land surface temperature. J. Environ. Manage. 295, 113116. https://doi.org/10.1016/j.jenvman.2021.113116.
- Zargari, M., Mofidi, A., Entezari, A., Baaghideh, M., 2024. Climatic comparison of surface urban heat island using satellite remote sensing in Tehran and suburbs. Sci. Rep. 14, 643. https://doi.org/10.1038/s41598-023-50757-2.
- Zhao, J., Zhao, X., Liang, S., Zhou, T., Du, X., Xu, P., Wu, D., 2020. Assessing the thermal contributions of urban land cover types. Landsc. Urban Plan. 204, 103927. https:// doi.org/10.1016/j.landurbplan.2020.103927.
- Zhao, K., Ning, Z., Xu, C., Zhao, X., Huang, X., 2024. How do driving factors affect the diurnal variation of land surface temperature across different urban functional blocks? a case study of Xi'an, China. Sustainable Cities and Society. 114, 105738. https://doi.org/10.1016/j.scs.2024.105738.
- Zhou, W., Qian, Y., Li, X., Li, W., Han, L., 2014. Relationships between land cover and the surface urban heat island: seasonal variability and effects of spatial and thematic resolution of land cover data on predicting land surface temperatures. Landsc. Ecol. 29, 153–167. https://doi.org/10.1007/s10980-013-9950-5.
- Zhu, B., Cheng, Y., Hu, X., Chai, Y., Berghuijs, W.R., Borthwick, A.G., Slater, L., 2023. Constrained tropical land temperature-precipitation sensitivity reveals decreasing evapotranspiration and faster vegetation greening in CMIP6 projections. npj Clim. Atmos. Sci. 6, 91. https://doi.org/10.1038/s41612-023-00419-x.